



1 Regional temperature change potentials for short lived 2 climate forcings from multiple models

3 Borgar Aamaas¹, Terje K. Berntsen^{1,2}, Jan S. Fuglestad¹, Keith P. Shine³, William J.
4 Collins³

5 ¹CICERO Center for International Climate Research, PB 1129 Blindern, 0318 Oslo, Norway

6 ²Department of Geosciences, University of Oslo, Norway

7 ³Department of Meteorology, University of Reading, Reading RG6 6BB, United Kingdom

8 *Correspondence to:* Borgar Aamaas (borgar.aamaas@cicero.oslo.no)

9 **Abstract.** We calculate the absolute regional temperature change potential (ARTP) of various short lived climate
10 forcings (SLCFs) based on detailed radiative forcing (RF) calculations from four different models. The temperature
11 response has been estimated for four latitude bands (90-28° S, 28° S-28° N, 28-60° N, and 60-90° N). The regional
12 pattern in climate response not only depends on the relationship between RF and surface temperature, but also on
13 where and when emissions occurred and atmospheric transport, chemistry, interaction with clouds, and deposition.
14 We present four emissions cases covering Europe, East Asia, the global shipping sector, and the globe. Our study
15 is the first to estimate ARTP values for emissions during Northern Hemisphere summer (May-October) and winter
16 season (November-April). The species studied are aerosols and aerosol precursors (black carbon (BC), organic
17 carbon (OC), SO₂, NH₃), ozone precursors (NO_x, CO, volatile organic compound (VOC)), and methane (CH₄).
18 For the response to BC in the Arctic, we take into account the vertical structure of the RF in the atmosphere, and
19 an enhanced climate efficacy for BC deposition on snow. Of all SLCFs, BC is the most sensitive to where and
20 when the emissions occur, as well as giving the largest difference in response between the latitude bands. The
21 temperature response in the Arctic is almost 4 times larger and more than 2 times larger than the global average
22 for Northern Hemisphere winter emissions for Europe and East Asia, respectively. The latitudinal breakdown gives
23 likely a better estimate of the global temperature response as it accounts for varying efficacies with latitude. An
24 annual pulse of non-methane SLCFs emissions globally (representative of 2008) leads to a global cooling. Whereas,
25 winter emissions in Europe and East Asia give a net warming in the Arctic due to significant warming from BC
26 deposition on snow.

27 1 Introduction

28 Climate is influenced by a multitude of emissions with varying impacts (e.g., Myhre et al., 2013). Emissions of
29 short lived climate forcings (SLCFs), such as black carbon (BC), organic carbon (OC), SO₂, NH₃, NO_x, CO, and
30 volatile organic compounds (VOCs), affect the composition of the atmosphere primarily on time scales of days to
31 a few months. CH₄ is often also included because its lifetime of around 10 years is shorter than or comparable to
32 climate response timescales. The temporal variation in the geographical pattern of SLCF emissions has changed
33 over time, with emissions typically being high in the early phases of industrialization, and then gradually being
34 reduced due to air quality concerns and technological improvements. Nevertheless, emissions are still growing in
35 many parts of the world, and there is a growing focus politically to develop mitigation strategy for the SLCFs to



36 achieve both improved air quality and slowing global warming (Schmale et al., 2014; Shindell et al., 2012; Stohl et
37 al., 2015).

38 Due to the short atmospheric lifetimes, emissions of SLCFs lead to a spatial pattern in radiative forcing (RF) that
39 is more inhomogeneous than for emissions of long-lived greenhouse gases such as CO₂. It is well established that
40 there is not a close relationship between the RF pattern and the surface temperature response pattern, due to
41 modifications by heat transport in the atmosphere and ocean and the spatial variability in climate feedbacks (e.g.,
42 Boer and Yu, 2003). However, as shown by Shindell and Faluvegi (2009) and Shindell (2012), it is possible to
43 establish relationships between the RF pattern caused by a certain component and the response in broad latitude
44 bands. Recently, Najafi et al. (2015), have shown from observational and model data that there is a distinct
45 difference in the Arctic response to the overall forcing by ozone, aerosols and land-use, compared to other latitude
46 bands.

47 Emission metrics are simple tools based on comprehensive model simulations that relate emissions to a certain
48 response (physical climate change or economic damage), e.g. Fuglestedt et al. (2003); Tol et al. (2012). The most
49 widely used emission metric, the Global Warming Potential (GWP), is given by the integrated RF (over a time
50 horizon of H years) in response to a pulse emission. Shine et al. (2005) introduced the Global Temperature change
51 Potential (GTP), using the surface temperature change (after a time horizon of H years) for the response. Emissions
52 metrics have typically estimated a global effect due to global emissions (e.g., Aamaas et al., 2013). A first step
53 going beyond global means was to quantify the global response based on regional emissions for SLCFs (Berntsen
54 et al., 2005; Wild et al., 2001; Stevenson et al., 2004; Fuglestedt et al., 2010; Collins et al., 2013; Aamaas et al.,
55 2016; Fry et al., 2012). By introducing the concept of regional temperature potentials (RTP), Shindell and Faluvegi
56 (2010) extended the metric concept to include regional responses (in terms of surface temperature change in broad
57 latitude bands) to regional emissions.

58 In addition to the regionality, the timing of the SLCFs emissions matter. This is potentially important since the
59 photochemistry in the atmosphere, lifetime, atmospheric transport and forcing efficiency is likely to vary between
60 the seasons. As some sources (e.g. domestic heating and agricultural waste burning) have a large seasonal cycle,
61 using seasonal RTP metrics might have a significant impact on the evaluation of cost-effectiveness of mitigation
62 measures.

63 Here we use detailed multimodel calculations of the relationship between emission location and the resulting
64 specific RF (RF per Tg/yr emissions) for SLCFs (Bellouin et al., 2016) (Sect. 2.1) and the regional climate
65 sensitivities (e.g., Shindell and Faluvegi, 2009) to estimate ARTPs for a range of aerosols, aerosol precursors, and
66 ozone precursors (BC, OC, SO₂, NH₃, NO_x, CO, and VOC), and CH₄ (Sect. 2.2). While some of our findings
67 confirm the results by Collins et al. (2013), our analysis build on that work in several ways (see also Aamaas et
68 al., 2016). Our study is the first to calculate ARTPs for NH₃ emissions. The treatment of BC in the Arctic is more
69 complex which has a high influence on the ARTPs for BC. Aspects of the aerosol effects on ozone precursors are
70 also novel. For the first time, we distinguish between ARTPs for emissions taking place during Northern
71 Hemisphere (NH) summer (May-October) and winter (November-April). ARTP metrics are calculated for regional
72 emissions from Europe, East Asia and the shipping sector, as well as global emissions (Sect. 3.1). The ARTP



73 values are applied to global emissions in Sect. 3.2. We also make a comparison of ARTPs with AGTPs (Sect. 3.3).
74 Uncertainties are discussed in Sect. 3.4, and we conclude in Sect. 4.

75 2 Material and methods

76 2.1 Radiative forcing

77 The RFs that are the basis for the ARTP calculations of the SLCFs are calculated using 4 different chemistry
78 climate models or chemical-transport models presented by Bellouin et al. (2016); see details about the models in
79 Table 1. RFs are produced based on a control simulation and numerous perturbation simulations that consider a
80 20% emission reduction in one type of species and one region in NH summer or winter. The ECLIPSE emission
81 dataset applied here was created with the GAINS (Greenhouse gas-Air pollution Interactions and Synergies) model,
82 see Stohl et al. (2015). The regional pattern of the RFs is taken into consideration with four latitude bands, southern
83 mid-high latitudes (90-28° S), the Tropics (28° S-28° N), northern mid-latitudes (28-60° N), and the Arctic (60-
84 90° N), as forcing-response coefficients are only available for those latitude bands in the literature (e.g., Shindell
85 and Faluvegi, 2010;Shindell, 2012).

86 We compute ARTPs for six different processes that contribute to the RF for each species (see Fig. 1 for details).
87 The quantification of these processes are given by the RF data from Bellouin et al. (2016). For the general
88 circulation models, the RFs of the aerosol perturbations are calculated online using two calls to the radiation
89 scheme. This method involves diagnosing radiative fluxes with and without the perturbation. These RFs do not
90 include rapid adjustments (even in the stratosphere). For the OsloCTM2 chemistry transport model and the RF
91 exerted by the ozone precursors in all the models, RF is computed by offline radiative transfer codes. The RF for
92 methane is based on the analytical expression that includes stratospheric adjustments (Myhre et al., 1998), which
93 gives a global mean. Based on this global RF estimate, we apply the latitudinal pattern in RF for methane and
94 methane induced ozone response in Collins et al. (2013). This pattern is based on an ensemble of 11 global
95 chemical transport models that evaluated a global reduction of CH₄ mixing ratio, where RF was calculated using
96 the method developed by the NOAA Geophysical Fluid Dynamics Laboratory (Fry et al., 2012).

97 For aerosols and aerosol precursors, all four models calculate the aerosol direct and 1st indirect (cloud-albedo)
98 effect, except ECHAM6 which only includes direct RF. In this study, we group together the aerosol direct and 1st
99 indirect (cloud-albedo) effect and name this process *aerosol effects*. In addition, OsloCTM2 estimated the RF from
100 BC deposition on snow and the semi-direct effect. The semi-direct effect is quantified in Bellouin et al. (2016) by
101 prescribing control and perturbed distributions of BC mass-mixing ratios in the CAM4 model and using 30-year
102 simulations with fixed sea-surface temperatures to suppress the long-term response. For the ozone precursors and
103 CH₄, the total RF takes into account the aerosol direct and 1st indirect effects, short-lived ozone effect, methane
104 effect, and methane-induced ozone effect. Only OsloCTM2 includes an estimate for nitrate aerosols, which is
105 added to the *aerosol effect* quantification in the other models.

106 The best estimate of a species' RF has been calculated as the sum of all processes, in which the average across the
107 models is used for each process. Not all models have estimated RFs for all species and processes. In addition,
108 ECHAM6 is excluded in the best estimate for BC, OC, and SO₂, since it did not estimate the 1st indirect effect. For
109 BC deposition on snow, the BC semi-direct effect, and nitrate aerosol, the best estimate is solely based on the



110 OsloCTM2 model, while the best estimate are based on three models for all other processes (*aerosol effects*, short-
111 lived ozone, methane, and methane-induced ozone).

112 For the high and low estimates of RF for each emission case, we find these values by taking the sum of the highest
113 and lowest values, respectively, from all models for each individual process.

114 The emission regions are defined according to tier1 Hemispheric Transport of Air Pollution (HTAP) regions (see
115 Bellouin et al., 2016). Europe is defined as Western and Eastern Europe up to 66°N including Turkey. East Asia
116 includes China, Korea, and Japan. Shipping is the global shipping sector. The global emissions category excludes
117 this shipping activity. As RF values are also available for the remaining land areas outside of Europe and East
118 Asia, results from the rest of the World are presented in SI Sect. 2.

119 2.2 Regional temperature change potentials

120 The regional temperature response has been calculated on the basis of RF in the latitude bands and regional climate
121 sensitivities, as well as the temporal evolution of an idealized temperature response. Even though our estimates
122 are based on seasonal emissions, the temperature responses calculated are annual means. The general expression
123 for the ARTP following a pulse emission of component i (E_i) in region r which leads to a response in latitude
124 band m is (e.g., Collins et al., 2013):

$$125 \text{ARTP}_{i,r,m,s}(H) = \sum_l \int_0^H \frac{F_{l,r,s}(t)}{E_{i,r,s}} \times RCS_{i,l,m} \times R_T(H-t) dt \quad (1)$$

126 $F_{l,r,s}(t)$ is the RF in latitude band l due to emission in region r in season s as a function of time (t) after the pulse
127 emission $E_{r,s}$ (in Tg). The $RCS_{i,l,m}$ is a matrix of regional response coefficients based on the RTP concept (unitless,
128 cf. Collins et al., 2013). As these response coefficients are here normalized, they contain no information on climate
129 sensitivity, only the relative regional response pattern. The global climate sensitivity is included in the impulse
130 response function R_T , which is a temporal temperature response to an instantaneous unit pulse of RF (in $\text{K}/(\text{Wm}^{-2})$).
131 We assume that the time evolution of temperature in each response band follows the global-mean time
132 evolution. We base our temperature response on that of the HadCM3 climate model (Boucher and Reddy, 2008)
133 with an equilibrium climate sensitivity of $1.06 \text{ K}/(\text{W m}^{-2})$, which translates to a 3.9 K warming for a doubling of
134 CO_2 concentration. This is the same climate sensitivity as for our absolute Global Temperature change Potential
135 (AGTP) calculations on the same RF dataset (Aamaas et al., 2016).

136 Regional temperature responses of an emission scenario $E(t)$ can be calculated with these ARTP values by a
137 convolution (see also Aamaas et al., 2016). The temperature response is:

$$138 \Delta T_i(t) = \int_0^t E_i(t') \times \text{ARTP}_i(t-t') dt' \quad (2)$$

139 2.2.1 For species with lifetimes less than one year

140 For SLCFs with atmospheric lifetimes (or indirect effects causing RF) much shorter than both the time horizon of
141 the ARTP and the response time of the climate system (given by the time constants in R_T above), the general
142 expression for the ARTP can be simplified to:

$$143 \text{ARTP}_{i,r,m,s}(H) = \sum_l \frac{F_{l,r,s}}{E_{i,r,s}} \times RCS_{i,l,m} \times R_T(H) \quad (3)$$



144 $F_{l,r,s}$ is the RF over a year where emissions of component i ($E_{i,r,s}$ in Tg/yr) in emission region r occur during season
145 s , either during NH summer or winter.

146 2.2.2 For species that affect methane

147 Methane has an adjustment time comparable to the time horizon of the ARTP and the response time of the climate
148 system. So, for species that affect methane, an additional impulse response function that describes the atmospheric
149 decay of methane must be included (R_F). In this case, we add such a function, which governs the methane and
150 methane-induced ozone effects for the ozone precursors (NO_x, CO, and VOC) and CH₄.

$$151 R_F(t) = e^{-t/\tau}, \quad (4)$$

152 where $\tau=9.7$ yr is the average adjustment time for methane in the three models. For these species, this additional
153 temperature perturbation due to these processes has to be included:

$$154 ARTP(R_F \text{ response})_{i,r,m,s}(H) = \sum_l \int_0^t \frac{F_{l,i,r,s}}{E_{i,r,s}} \times R_F(H-t) \times RCS_{i,l,m} \times R_T(H-t) dt \quad (5)$$

155 2.2.3 Forcing-response coefficients

156 The unitless regional sensitivity matrix ($RCS_{i,l,m}$) is estimated based on literature values of regional response
157 coefficients in K/(W m⁻²) (see Sect. 1 in Supporting Information for tabulated coefficients). All these response
158 coefficients from the different literature sources have been normalized to the global response in those studies.
159 While the specific regional response coefficients have been estimated in other studies based on climate sensitivities,
160 the normalization to the global response removes the implicit climate sensitivities in the RCS values. We do several
161 adjustments and refinements of the RCS values (see this section and Sect. 2.2.4); in each case, we normalize the
162 response coefficients and make sure that the climate sensitivity in our ARTP calculations are only incorporated in
163 R_T .

164 As such, RCS matrices only exist for annual emissions, we assume we can apply the same set of matrices for
165 emissions during NH summer and winter. For the scattering aerosols and aerosol precursors (SO₂, OC, NH₃), we
166 use the coefficients tabulated in Shindell and Faluvegi (2010), which are the mean responses of CO₂ and SO₂. The
167 same values are used for the long-lived effects (methane and methane-induced ozone) of the ozone precursors and
168 CH₄. For the short lived effects of the ozone precursors and CH₄, we apply the O₃ coefficients in Shindell and
169 Faluvegi (2010) as tabulated in Collins et al. (2013).

170 For BC, the regional sensitivity matrix is based on several sources, and the details for the Arctic-to-Arctic
171 responses are described in Sect. 2.2.4. For other latitude bands, the matrix for the *aerosol effects* is given by BC
172 forcing-response coefficients from Shindell and Faluvegi (2009) as tabulated in Table 3 in Collins et al. (2013)
173 and the matrix for the semi-direct effect is from the CO₂ coefficients shown in Shindell and Faluvegi (2010) based
174 on Shindell and Faluvegi (2009). The semi-direct effect can potentially be included either in the response based
175 on RCS values or in the RF. Our approach is to include the semi-direct effect in the RF and not in the RCS values,
176 see next paragraph for details. The relationship for the deposition of BC on snow is also given by the CO₂
177 coefficients shown in Shindell and Faluvegi (2010). For the snow albedo effect, we have assumed an efficacy of
178 3 for all RF occurring outside of the Arctic (Myhre et al., 2013).



179 Our method differs from Shindell and Faluvegi (2009) as we have calculated the semi-direct effect independently.
180 Since Shindell and Faluvegi (2009) did not have any rapid adjustments in their sensitivities on RFs, the rapid
181 adjustments are implicitly included in their sensitivity coefficients. The reason is that in the GCM simulations used
182 to calculate the forcing-response coefficients (Shindell and Faluvegi, 2009; Flanner, 2013), semi-direct effects are
183 treated as feedbacks and as such they are included in the forcing-response coefficients. When we normalize to the
184 global response to find the RCS coefficients, we normalize on the global CO₂ response given by Shindell and
185 Faluvegi (2009) for all the species to avoid double counting.

186 **2.2.4 Refinement of Arctic Response to BC**

187 We do two refinements of the forcing-response coefficients for RFs occurring in the Arctic, one for the *aerosol*
188 *effects* in the atmosphere and one for the effects due to BC on snow. We first discuss how we handle the *aerosol*
189 *effects* in the atmosphere.

190 For BC in the Arctic, the forcing by absorption takes place in a generally stably stratified atmosphere. The transport
191 of BC to the Arctic occurs approximately along isentropic surfaces; thus emissions from East Asia are generally
192 at a higher altitude than emissions from Europe. The BC particles cause also dimming at the surface. In the Arctic,
193 heat is not easily mixed down to the surface. The efficacy of BC forcing depends highly on the altitude of the BC
194 (Flanner, 2013; Lund et al., 2014; Sand et al., 2013). To account for this the RTP concept is modified for BC forcing
195 in the Arctic. The contribution by RF exerted in the three latitude bands outside the Arctic to Arctic warming
196 ($ARTP(ex-Arc)_{BC,r,Arc,s}$) is calculated with the standard method using RTP-coefficients from Shindell and Faluvegi
197 (2010), as described in Sect. 2.2.3:

$$198 \quad ARTP(ex - Arc)_{BC,r,Arc,s}(H) = \sum_{l=1}^3 \frac{F_{l,BC,r,s}}{E_{BC,r,s}} \times RCS_{BC,l,Arc} \times R_T(H) \quad (6)$$

199 For the RF within the Arctic the response ($ARTP(Arc)_{BC,r,Arc,s}$) is calculated according to Eq. (7) following the
200 method presented in Lund et al. (2014):

$$201 \quad ARTP(Arc)_{BC,r,Arc,s}(H) = \sum_z \frac{F^{(z)}_{Arc,BC,r,s}}{E_{BC,r,s}} \times RCS(z)_{BC,Arc,Arc} \times R_T(H) \quad (7)$$

202 Both the RF ($F^{(z)}_{Arc,BC,r,s}$) and the regional sensitivity matrix ($RCS(z)_{BC,Arc,Arc}$) have a dependence on the height of
203 the BC which is denoted by the z in Eq. (7). We apply a vertically-resolved regional sensitivity matrix based on
204 Fig. 2(a) in Lund et al. (2014), which shows the sensitivity of the Arctic surface temperature response to the altitude
205 of RF in the Arctic from Flanner (2013) interpolated to the vertical structure in OsloCTM2. This relationship can
206 be combined with the normalized BC RF from Samset and Myhre (2011) to give a normalized Arctic surface
207 temperature response to BC perturbations at different altitudes.

208 We apply the vertical profile of BC concentration in the Arctic for all three models used. These vertical profiles
209 are converted into RF profiles based on the vertically resolved RF to burden ratio in OsloCTM2.

210 Our second refinement is on the forcing-response coefficients for BC on snow in the Arctic, where we use the
211 forcing-response sensitivity found by Flanner (2013).

212 As the semi-direct effect is implicitly included in the estimates from Flanner (2013), we cannot distinguish between
213 direct RF and semi-direct RF for RF occurring in the Arctic. The Arctic RF due to the semi-direct effect provided



214 in Bellouin et al. (2016) is left out to avoid double counting. However, our argument is that the explicit vertically
215 resolved forcing-response relationships is a much better fit than a vertically averaged forcing-response
216 relationships, which makes this the preferable method. As a result, this study's ARTP estimates of the semi-direct
217 effect in the Arctic is due to the semi-direct RF from outside the Arctic.

218 The Flanner (2013) study is based on an equilibrium climate sensitivity of $0.91 \text{ K}/(\text{W m}^{-2})$, which is 14% lower
219 than applied in our study. We adjust our calculations so that the climate sensitivity is in line with the rest of our
220 calculations (Boucher and Reddy, 2008). The correction is done with a two-layer box-diffusion model based on
221 the parameters of the Hadley Centre model (see Aamaas et al., 2013), which also modifies the timescales of the
222 impulse response function.

223 The total response in the Arctic is then the sum of the contributions from BC forcing outside of the Arctic and
224 inside of the Arctic.

$$225 \quad \text{ARTP}_{BC,r,Arc,s}(H) = \text{ARTP}(ex - Arc)_{BC,r,Arc,s}(H) + \text{ARTP}(Arc)_{BC,r,Arc,s}(H) \quad (8)$$

226 **3 Results**

227 **3.1 ARTP values**

228 **3.1.1 Best estimates** 229 **Results for ARTP(20)**

230 The best estimates of ARTP values for a time horizon of 20 years are presented in Fig. 1, for each of the four
231 emission regions, the four response bands, plus the global mean, for all emitted species considered here. We
232 provide values for other time horizons (10, 50 and 100 years) in Supporting Information Sect. 2. The rationale for
233 highlighting 20 years is that if the focus is to be placed on mitigation of SLCFs then it is more appropriate to
234 investigate climate impacts on short timescales. Continuous time horizons between 1-50 years are given in Sect.
235 3.1.5.

236 The uncertainties in Fig. 1 are given as a range following the differences in RFs estimated between the models.
237 We acknowledge other uncertainties, such as for climate sensitivity, which are discussed in Sect. 3.4. The
238 uncertainty is often larger than the variation between different emission regions, seasons, and responses in the
239 latitude bands. However, we will show in Sect. 3.1.4 that the relative variations between the best estimates for
240 individual species are often robust. As ARTP values for the shipping sector are based on only two RF estimates,
241 uncertainty ranges are not given for shipping. The robustness in the best estimate for shipping is likewise lower
242 than for the other regions. E.g., these two models disagree for shipping on the sign for the *aerosol effect* of NO_x
243 emissions. NH_3 estimates are also from one model only, and are not shown for shipping (because emissions from
244 that sector are negligible).

245 **Response patterns**

246 For emissions from a given region, the latitudinal response pattern is partly governed by the pattern of RF and
247 partly the pattern in the forcing-response coefficients. The RF signal is mainly located in the latitude bands near
248 the emission sources for the short-lived components, while it is more evenly distributed for processes linked to



249 methane. Hence, as shown in Bellouin et al. (2016) (see especially their Fig. 7), emissions in Europe and East
250 Asia give largest RF in the NH mid-latitude band and the smallest in the Southern Hemisphere (SH) mid-high
251 latitudes. Due to heat transport between the latitude bands and the temperature response lasting over several years,
252 the forcing-response is averaged out over several latitude bands by the temperature response. Nevertheless, the
253 temperature response has higher sensitivity towards the Arctic and NH mid-latitude bands (see all panels in Fig.
254 1) as a result of local feedback processes being stronger in the Arctic, driven by local cloud, water vapor, and
255 surface albedo feedbacks (Boer and Yu, 2003).

256 We next consider differences between the emission regions Europe and East Asia. The RF per unit emission is
257 dependent on where the emissions occur, which causes differences in the ARTP(20) values. The differences in the
258 global average of RFs and global emission metric values such as AGTP(20) are discussed in Aamaas et al. (2016).
259 In short, the emission metric values for the aerosols are larger for European than East Asian emissions, but not for
260 NH₃ in winter. Variations are also seen for the ozone precursors, but these differences are relatively smaller
261 between European than East Asian emissions for CO and VOC than for the aerosols. For CO, East Asia has
262 marginally larger values (see Figs. 1(K) and 1(L)) and marginally larger for European VOC emissions (see Figs.
263 1(M) and 1(N)). The main difference in the global average of ARTP values calculated here and the AGTP values
264 calculated in Aamaas et al. (2016) is the much larger impact for BC deposition on snow for ARTP (see Fig. 1(B)),
265 as the AGTP study did not account for the increased efficacy of BC deposition on snow.

266 The timing of emissions also influences the RF per unit emissions. The emission metric values for the aerosol
267 emissions in Europe and East Asia (see Figs. 1(A)-1(F)) are larger for summer than winter, except for BC. For the
268 aerosols, the aerosol RF is driven by seasonal variations in the incoming solar radiation. More sunlight in local
269 summer results in stronger RFs (Bellouin et al., 2016). Seasonal differences in atmospheric lifetimes due to
270 seasonality in precipitation may also contribute. BC is discussed in detail in Sect. 3.1.2.

271 For the ozone precursors (see Figs. 1(I)-1(N)), the largest values occur in winter for CO (Figure 1(L)) and in
272 summer for VOC (Figure 1(M)). CO has a longer lifetime during local winter leading to a larger fraction of the
273 CO emitted being transported from the higher latitudes to the Tropics. Here, the effects of CO-oxidation on tropical
274 OH have the largest impacts on the methane lifetime.

275 The latitudinal response patterns are similar for the different species. For all the species, the response bands with
276 the largest ARTP values are for the responses in the NH mid-latitudes (60% of the cases) and Arctic and the band
277 with the least response the SH mid-high latitudes (see all panels in Fig. 1). This skewness is partly due to the
278 emissions occurring mainly in the NH, but the same pattern is seen for CH₄ (Figure 1(O)), for which the emission
279 location is less important. Further, the high ARTP values for the Arctic are also due to stronger local feedback
280 processes, leading to larger forcing-response sensitivities, while high ARTP values for the NH mid-latitudes are a
281 combination of high RF values per unit emission and relatively large regional climate sensitivities. The low ARTP
282 values for SH mid-high latitudes is caused by a combination of most emissions occurring in NH and weaker
283 forcing-response coefficients in SH. Let us consider OC emissions in East Asia during summer as an example with
284 RF mostly in one band. The RF (see Bellouin et al., 2016) in the NH mid-latitude band is 260% above the global
285 average, practically zero in the SH mid-high latitude band and about 50% below the global average in the other
286 two bands. This skewedness is also modeled in the ARTP (see Fig. 1(C)), but with more emphasis on the Arctic.



287 The ARTP value for the responses in the Arctic and NH mid-latitudes is about 70% and 90% above the global
288 average, respectively. In the SH mid-high latitudes response band, the ARTP value is about 20% of the global
289 average. At the other end of the range, emissions of CH₄ have a global impact due to the atmospheric lifetime of
290 CH₄ (9.7 years). The RF in the Arctic band is 35% below the global average, while 25% above in the Tropics. But
291 the weighing is almost opposite for the ARTP, as the Arctic response band has a ARTP value 34% above the global
292 average and the Tropics 13% above the average (see Fig. 1(O)). For the SH mid-high latitude response band, both
293 the RF and ARTP are lower than the global average, by -35% and -49%, respectively.

294 For most of the aerosol emissions (see Figs. 1(A)-1(F)), the ARTP values for the *aerosol effects* component are
295 larger for emissions in NH summer than winter, even in the Tropics for emission from both Europe and East Asia.
296 The only exception is NH₃ (Figures 1(G) and 1(H)), which has a larger ARTP value for winter than summer for
297 East Asian and global emissions. Longer sunlight duration in the summer hemisphere yields stronger RFs (Bellouin
298 et al., 2016), which impact the ARTP value for the response even in the Tropics. This general observation does
299 not hold for BC when we include the process “BC deposition on snow”, as this process is largest in NH winter.

300 The ARTP(20) values shift sign for some of the latitude response bands. VOC emissions generally lead to a
301 warming, however, our best estimate indicates a small cooling in SH mid-high latitudes for European and East
302 Asian winter emissions (Figure 1(N)). The negative RF for the *aerosol effect* in this response band is driving this
303 cooling as the other perturbations have a small impact on the response in the SH mid-high latitudes. For the ozone
304 precursors, the *aerosol effects*, and the short-lived ozone effect to a smaller degree, also shift between warming
305 and cooling depending on the latitude response band.

306 3.1.2 Variation of BC response with emission season and region

307 The largest differences in ARTP(20) values are seen for BC, such as the timing of emissions (comparing Figs. 1(A)
308 and 1(B)) and the location during winter (comparing the different emission regions in Fig. 1(B)).

309 The total emission metric values of BC emissions depend on which processes are included. The direct *aerosol*
310 *effect* is larger for summer than winter emissions. The direct temperature response is similar for emissions
311 occurring in Europe, East Asia, and globally. Similarly, the semi-direct effect is most pronounced in summer as
312 this effect is driven by absorption of shortwave radiation. When the influence from the BC deposition on snow is
313 included, the ARTP value increases significantly for emissions during NH winter. For emissions in Europe, the
314 global temperature response to the semi-direct effect is -46% and -12% of the *aerosol effect* in summer and winter,
315 respectively, and the deposition on snow effect 12% and 230% of the *aerosol effect* in summer and winter,
316 respectively. The relative share of the deposition on snow effect is 60 % lower for winter East Asian emissions
317 than for winter European emissions. The semi-direct effect has a relative weight of -56% compared to the *aerosol*
318 *effect* for the global ARTP(20) East Asian emissions in summer and close to zero in winter. The impact of BC
319 deposition of snow is largest when large snow and ice covered surface areas and solar radiation at the BC
320 deposition location is combined, such as in late winter. The response from European emissions is larger than for
321 East Asian emissions since the emission region is closer to the Arctic, which makes BC transport into the sensitive
322 Arctic more likely (Sand et al., 2013). The effect of the BC deposition on snow dominates the winter-summer
323 difference for BC and hence our results are sensitive to both the calculated RF and efficacy for this BC process.



324 The Arctic response amplification, i.e., how much stronger the response is in the Arctic relative to the global
325 average, is largest for winter emissions as the deposition on snow effect is relatively larger than for summer
326 emissions. The total Arctic response amplification for BC is for European emissions 240% and 390% larger than
327 the global average in summer and winter, respectively, and for East Asian emissions 160% and 240% larger than
328 the global average in summer and winter, respectively. As a result, wintertime BC emissions have the largest
329 latitudinal variation in the ARTP(20) for all SLCFs. This Arctic amplification is driven by the temperature response
330 from deposition on snow effect (almost 500% for European emissions and 400% for East Asian emissions for this
331 process), which is largest in the Arctic response band, above the global average in the NH mid-latitude, and below
332 average in the two other response bands. Latitudinal response variations are also found for the other processes, but
333 relatively much smaller.

334 3.1.3 Comparison with Collins et al. (2013)

335 Our findings are largely consistent with those by Collins et al. (2013). Similarities occur because the two studies
336 share some of the same forcing-response coefficients and climate sensitivity (Boucher and Reddy, 2008). In this
337 work, we have a more detailed treatment of BC in the Arctic and we include NH₃, as well as more detailed for
338 aerosol impacts on ozone precursors. ARTP values are also given for two seasons, for the shipping sector and our
339 global estimate include all emissions.

340 The ARTP(20) values in Collins et al. (2013) are mostly lower than the average response of annual emissions in
341 this study, while the variations between the latitude response bands are mostly similar. We model 180% and 80%
342 stronger global temperature sensitivity from European and East Asian emissions of BC. The largest difference is
343 that our study included the response from BC deposition in snow. In addition, Collins et al. (2013) applied a
344 forcing-response coefficient for the BC direct RF that gives an Arctic cooling due to emissions in the Arctic
345 (Shindell and Faluvegi, 2009). When including a more detailed parameterization for atmospheric BC in the Arctic
346 that considers the height of the BC (see Sect. 2.2.4), the global temperature response of BC emissions increases
347 by 4-14%. The difference is much larger in the Arctic, and the increase in the Arctic is 22-210% when only
348 considering the BC direct and 1st indirect effects.

349 3.1.4 Robustness for individual species

350 The differences between ARTP(20) values for different emission regions and emission seasons, as well as for the
351 response in different latitude bands for one set of emissions, are smaller than the inter-model uncertainty ranges.
352 However, the ARTPs based on RFs for the individual models agree often with the best estimate on the ranking
353 between the different emission and response cases, which strengthens our confidence that the variations calculated
354 for the best estimate are robust. In Supporting Information Sect. 3, we quantify this robustness and find a high
355 robustness consistent with similar analysis done on AGTP(20) values (Aamaas et al., 2016). As the temperature
356 response is more smeared out globally for the ozone precursors than for the aerosols, the models agree to a larger
357 extent for the aerosols concerning which latitude response bands see the largest and smallest temperature
358 perturbations. For BC, we compare results only including the *aerosol effects* as only one model includes BC on
359 snow and semi-direct effects. The model NorESM has the largest discrepancy relative to the best estimate for NO_x
360 and VOC, while HadGEM3 disagree the most for CO.



361 **3.1.5 Variations with time horizon**

362 We have so far only analyzed ARTP(20) values. Here we present results for a range of time horizons up to 50
363 years in Fig. 2. The ARTP values vary greatly with time horizon and generally decrease in magnitude with time
364 for SLCFs, especially for the aerosols (see Figs. 2(A) and 2(B) for BC). The ranking between different regions,
365 seasons and latitude bands also changes with varying time horizon for the ozone precursors (see Figs. 2(C)-2(H)).
366 The reason is that the aerosols and aerosol precursors have atmospheric lifetimes of about a week, while methane
367 has an atmospheric perturbation lifetime of almost 10 years, which will lead to variations in the relative weight of
368 the short-term and long-term processes with varying time horizons for the ozone precursors (e.g., Collins et al.,
369 2013).

370 The temporal variability shows that NO_x emissions in Europe have the most negative ARTP values for summer
371 than for winter for all time horizons, which is due to a stronger methane effect (Figure 2(C)). For East Asian
372 emissions, the situation is mixed with the most negative ARTP values in the first 10-15 years for winter emissions,
373 while summer emissions have the most negative values for longer time horizons (Figure 2(D)). For summer
374 emissions, ARTP values in the first few years is pushed upwards by stronger solar insolation than in winter leading
375 to more short-lived ozone. For the ozone precursors, the ranking on which latitude band is the most sensitive is
376 mostly unchanged after 5 years, but can vary in the first years.

377 **3.2 Regional temperature response for 2008 emissions**

378 Given the ARTP values, we calculate the regional and global temperature responses due to real-world emissions
379 of SLCFs. The temperature response at time H in latitude band m for an emission E of species i is

$$380 \Delta T_{i,r,m,s}(H) = E_{i,r,s} \times ARTP_{i,r,m,s}(H) \quad (9)$$

381 We estimate the temperature response in the four latitude bands for a time horizon of 20 years given real-world
382 emissions in 2008 from Europe, East Asia, the shipping sector, and globally (Klimont et al., In prep.). The global
383 emissions are given in Supporting Information Table S7. Such a view on regional responses is useful as regional
384 variations will be hidden in the global mean response (e.g., Lund et al., 2012). The emissions include seasonal
385 variability with emissions often being largest in the NH winter season. The temperature perturbations are mainly
386 governed by the ARTP(20) values given in Sect. 3.1.1, but also by the seasonal cycle of the emissions. The
387 emissions in Europe and East Asia are larger in winter than summer for all species except NH₃, driven by larger
388 residential heating and cooking emissions during winter conditions. BC emissions are about 70% larger, OC
389 emissions 70-100% larger, and SO₂ emissions almost 20% larger in East Asia and more than 40% larger in Europe
390 (Klimont et al., In prep.). The seasonal variability is smaller for the ozone precursors, CO with the largest range
391 (43% more in winter).

392 For the global source region, ignoring the seasonality by applying annually averaged emissions and ARTP values
393 gives similar total temperature responses as treating the seasons separately and then averaging (differences of 0-
394 3%). However, when treating Europe or East Asia individually seasonal information changes the temperature
395 estimates by up to 18%. The difference is largest for the aerosols. For Europe, the temperature response increases
396 by 8% for BC and decreases the cooling by OC by 10%. The largest relative changes are seen in the net temperature
397 perturbation of all SLCFs.



398 Figure 3 shows that the temperature perturbations are smallest for the SH mid-high response latitudes and largest
399 for the Arctic and NH mid-latitudes, as seen for ARTP(20). For most latitude response bands, SO₂ has the largest
400 impact, so the net effect of the seven SLCFs is a cooling in most of the cases. BC has the second largest impact
401 with a warming that is largest for winter emissions. The shipping sector is dominated by cooling from SO₂ and
402 NO_x (see Figs. 3(E) and 3(F)), while the other sectors have a much broader mix of species causing both heating
403 and cooling. However, NO_x can be both warming and cooling depending on emission metric choices. For ARTP(20)
404 applying sustained emissions, NO_x has a relatively smaller cooling impact and even contributes to warming in
405 some latitude bands for shipping emissions in summer (see Supporting Information Fig. S1).

406 Emission of SLCFs lead normally to net cooling or effects that cancel each other out. However, we show that some
407 specific cases cause warming in the Arctic (see Figs. 3(B), 3(D), and 3(H)). Winter emissions in Europe and East
408 Asia cause a warming in the Arctic and almost no net perturbation in the NH mid-latitudes and other bands. The
409 main reason is the strong heating from the BC deposition on snow for winter emissions close to snow and ice
410 surfaces, as well as relatively larger BC emissions in winter than for the other species. For summer emissions in
411 Europe and East Asia (Figures 3(A) and 3(C)), the situation is the opposite with the largest cooling in the Arctic
412 and NH mid-latitudes. A small net heating in the Arctic is also observed for global emissions in the NH winter
413 season.

414 3.3 Global temperature response and comparing ARTP and AGTP

415 We discuss how adding complexity with four latitudinal response bands impacts the metric value by comparing
416 the global temperature response for regional and seasonal emissions presented in Sect. 3.2 based on ARTP with
417 the AGTP calculation in Aamaas et al. (2016). Shindell (2014) concluded that the efficacy of the temperature
418 response depends on the location of the RF. As a result, more RF in the NH middle to high latitudes for the aerosols
419 give a larger response than a globally averaged RF. Lund et al. (2012) found that an emission metric first based on
420 regional variations, then averaged globally gives a more complete and informative value than one based on global
421 mean inputs. Work by Stohl et al. (2015) shows that regional temperature estimates based on ARTPs mostly agree
422 with calculations with earth system models. Although heterogeneity can be better included in temperature
423 responses given by ARTPs compared to AGTPs, the superiority of ARTPs relative to AGTPs has not been tested
424 thoroughly and confirmed. However, we argue that the global temperature response can be better quantified with
425 ARTPs than AGTPs since a simple representation of varying efficacies due to heterogeneous RF is included.

426 How the global temperature responses are calculated given the AGTP values is shown in Supporting Information
427 Sect. 6 and Aamaas et al. (2016). For the ARTP values, the global temperature is calculated from the area-weighted
428 mean of the responses in the latitude bands. As the ARTP calculations are based on an efficacy of 3 for BC
429 deposition on snow, the same efficacy is applied in the AGTP calculations. Our comparison between the methods
430 applying ARTP and AGTP uses a pulse emission E . The difference in the global temperature perturbation ($\Delta T(\text{diff})$)
431 for species i between the two methods is then

$$432 \Delta T(\text{diff})_{i,r,s}(H) = \sum_m E_{i,r,m,s} \times \text{ARTP}_{i,r,m,s}(H) - E_{i,r,s} \times \text{AGTP}_{i,r,s}(H), \quad (10)$$

433 which is applied for each emission region r and emission season s .



434 We compare the temperature perturbation based on ARTP and AGTP for a time horizon of 20 years using the 2008
435 emissions. The largest difference is for NH summer emissions. For global NH summer emissions, ARTP(20) result
436 in 17% more net cooling than AGTP(20) and about 26% and 32% more cooling for European and East Asian
437 emissions, respectively. The differences in responses are smaller for NH winter emissions. Annually, global
438 emissions lead to a 13% larger cooling based on ARTP than on AGTP. See Sect. 7 in Supporting Information for
439 further details. The differences emerge because the patterns of RF and efficacy are correlated, with highest RFs
440 and highest efficacies in the northern mid latitudes and Arctic. Thus, the ARTPs are necessary even to obtain a
441 global temperature response since they account for these correlations.

442 Next, we analyze the differences between applying ARTP and AGTP for the individual species (see Fig. 4 and Fig.
443 S3 in Supporting Information). The relative differences are in most cases similar for the different emission regions
444 and seasons, which show that the differences between ARTP and AGTP are governed by differences in the forcing-
445 response coefficients between the two. The relative differences are generally larger for the aerosols than the ozone
446 precursors, as seen in Fig. 4, where only the emissions regions and seasons with a relative difference larger than
447 20% are presented. The temperature responses are generally stronger for the scattering aerosols and the BC
448 deposition on snow given the ARTP than the AGTPs, which is in line with greater efficacies due to rapid and
449 strong feedbacks for RFs in the northern mid-latitudes and the Arctic latitude bands (Shindell, 2014). BC and
450 ozone precursors are in general given lower weight when using ARTPs than AGTPs. Application of ARTP and
451 AGTP values give variation of up to 30% for individual processes, with an average of 12% for individual species.
452 ARTPs are more detailed in nature and through accounting for variations in efficacy will give more realistic global
453 temperature responses.

454 3.4 Uncertainties

455 The ARTP values calculated have uncertainties and limitations given by the uncertainties in each parameter on the
456 right hand side of Eq. (1). The uncertainty ranges shown in Fig. 1 are based on the range in $\frac{F_{Li}(t)}{E_i}$ across all
457 contributing models. Bellouin et al. (2016) point out four important aspects regarding model diversity. Lifetime
458 diversity is large, the unperturbed baseline causes diversity for non-linear mechanisms, the number of species
459 included varies among the models, and finally the strength of the interactions between aerosols and chemistry
460 differs among the models. The climate sensitivity included in R is 3.9 K for a doubling of CO₂ concentration
461 (Boucher and Reddy, 2008); however, IPCC (2013) estimate the climate sensitivity to likely be in the range 1.5-
462 4.5K. Uncertainty is also found in the time evolution of R_T . We have based this impulse response function on only
463 one model, while Olivié and Peters (2013) have shown that this will vary between models. For instance, they found
464 a spread in the GTP(20) value of black carbon of about -60 to +80% due to variability for R_T between models.
465 However, the uncertainty in R_T is less relevant for the regional patterns. The forcing-response coefficients are also
466 based mainly on one model (Shindell and Faluvegi, 2010). While we separate between emissions occurring during
467 NH summer and winter season, forcing-response coefficients do not exist on a seasonal basis. Hence, the seasonal
468 differences presented here in the ARTP values are not due to potential differences in the response sensitivities, but
469 due to differences in the RF. Aamaas et al. (2016) observed that estimates of $\frac{F_{Li}(t)}{E_i}$ tend to be correlated, which
470 increases the uncertainty when a mitigation package is considered.



471 Ideally, calculations of the temperature response of changed emissions of SLCFs should use earth system models
472 for the most correct estimates. However, this is extremely time consuming, and many emission perturbations will
473 have small signal/noise ratios. Users of emission metrics, such as policymakers and decision makers, might not
474 have the needed expertise to utilize advanced models. Although the ARTP calculations are simplifications and
475 contain uncertainties, these emission metrics are useful, simple, and quick approximations for calculating the
476 temperature response in the different latitude bands for emissions of single species or a mix of SLCFs.

477 **4 Conclusion**

478 We have presented ARTP values in four latitude bands (90-28° S, 28° S-28° N, 28-60° N, and 60-90° N) for
479 several SLCFs (BC, OC, SO₂, NH₃, NO_x, CO, VOC, and CH₄) based on four different models. Numbers are
480 provided for emission occurring in Europe, East Asia, from the global shipping sector, as well as globally.
481 Emissions were separated between the NH summer and winter seasons. Although ARTPs are simplifications, they
482 are useful for analyzing the temperature response to possible mitigation strategies. The ARTP values are largest
483 in the response bands Arctic and NH mid-latitudes and the smallest in the SH mid-high latitudes. The different
484 models agree in most of the cases on the ranking of the temperature perturbation in the different latitude bands.

485 BC is the species that is the most sensitive to the timing of emissions, to the location during winter, as well as
486 having the largest spread in responses between the latitude response bands in winter. The relative difference
487 between the response bands is largest for BC emissions during NH winter, and the more the closer to the Arctic
488 the emissions occur. The Arctic temperature response is 390% and 240% larger than the global temperature
489 response for winter emissions in Europe and East Asia, respectively. BC deposition on snow is the most important
490 process influencing the Arctic for BC emissions occurring in NH winter, both in absolute and relative terms.

491 We have also investigated how the global response based on ARTP compares with AGTP. Our study indicate that
492 the global temperature response can be better quantified with ARTPs than AGTPs since ARTPs include a simple
493 representation of varying efficacies due to heterogeneous RFs. For global emissions of SLCFs excluding CH₄,
494 calculations based on ARTP values give 13% larger cooling than based on AGTP values. Globally, both these
495 calculations based on ARTP(20) and AGTP(20) show a cooling, while European and East Asian winter emissions
496 give a small net warming or near zero impact according to ARTP. This is driven by net warming in the Arctic and
497 close to zero perturbation in the other latitude bands. For summer emissions, net cooling occurs in all latitude
498 bands, but are largest in the NH mid-latitudes and Arctic. Seasonal emissions and seasonal ARTP values give
499 almost the same total temperature response as annual emissions and annual ARTP values for global emissions, but
500 changes the temperature responses up to 18% when looking at emissions from regions such as Europe and East
501 Asia.

502 **Acknowledgements**

503 The authors would like to acknowledge the support from the European Union Seventh Framework Programme
504 (FP7/2007-2013) under grant agreement no 282688 – ECLIPSE, as well as funding by the Norwegian Research
505 Council within the project “the Role of Short-Lived Climate Forcers in the Global Climate Regime”. We thank
506 Nicolas Bellouin for providing RF data for all the models. In addition, we show our appreciation to Nicolas
507 Bellouin, Marianne Tronstad Lund, and Dirk Olivieé for giving us vertical distributions of BC in the Arctic.

508 **References**

- 509 Aamaas, B., Peters, G., and Fuglestedt, J. S.: Simple emission metrics for climate impacts, *Earth Syst. Dynam.*,
 510 4, 145-170, 10.5194/esd-4-145-2013, 2013.
- 511 Aamaas, B., Berntsen, T. K., Fuglestedt, J. S., Shine, K. P., and Bellouin, N.: Regional emission metrics for
 512 short-lived climate forcers from multiple models, *Atmos. Chem. Phys.*, 16, 7451-7468, 10.5194/acp-16-7451-
 513 2016, 2016.
- 514 Bellouin, N., Baker, L., Hodnebrog, Ø., Olivie, D., Cherian, R., Macintosh, C., Samset, B., Esteve, A., Aamaas,
 515 B., Quaas, J., and Myhre, G.: Regional and seasonal radiative forcing by perturbations to aerosol and ozone
 516 precursor emissions, *Atmospheric Chemistry and Physics*, 16, 13885-13910, 10.5194/acp-16-13885-2016, 2016.
- 517 Bentsen, M., Bethke, I., Debernard, J. B., Iversen, T., Kirkevåg, A., Seland, Ø., Drange, H., Roelandt, C.,
 518 Seierstad, I. A., Hoose, C., and Kristjánsson, J. E.: The Norwegian Earth System Model, NorESM1-M – Part 1:
 519 Description and basic evaluation of the physical climate, *Geosci. Model Dev.*, 6, 687-720, 10.5194/gmd-6-687-
 520 2013, 2013.
- 521 Berntsen, T., Fuglestedt, J. S., Joshi, M., Shine, K., Stuber, N., Li, L., Hauglustaine, D., and Ponater, M.:
 522 Climate response to regional emissions of ozone precursors: sensitivities and warming potentials, *Tellus B*, 57,
 523 283-304, 2005.
- 524 Boer, G. B., and Yu, B. Y.: Climate sensitivity and response, *Climate Dynamics*, 20, 415-429, 10.1007/s00382-
 525 002-0283-3, 2003.
- 526 Boucher, O., and Reddy, M. S.: Climate trade-off between black carbon and carbon dioxide emissions, *Energy*
 527 *Policy*, 36, 193-200, 2008.
- 528 Collins, W. J., Fry, M. M., Yu, H., Fuglestedt, J. S., Shindell, D. T., and West, J. J.: Global and regional
 529 temperature-change potentials for near-term climate forcers, *Atmos. Chem. Phys.*, 13, 2471-2485, 10.5194/acp-
 530 13-2471-2013, 2013.
- 531 Flanner, M. G.: Arctic climate sensitivity to local black carbon, *Journal of Geophysical Research: Atmospheres*,
 532 118, 1840-1851, 10.1002/jgrd.50176, 2013.
- 533 Fry, M. M., Naik, V., West, J. J., Schwarzkopf, D., Fiore, A., Collins, W. J., Dentener, F., Shindell, D. T.,
 534 Atherton, C. S., Bergmann, D. J., Duncan, B. N., Hess, P. G., MacKenzie, I. A., Marmer, E., Schultz, M. G.,
 535 Szopa, S., Wild, O., and Zeng, G.: The influence of ozone precursor emissions from four world regions on
 536 tropospheric composition and radiative climate forcing, *J. Geophys. Res.*, 117, D07306, 10.1029/2011JD017134,
 537 2012.
- 538 Fuglestedt, J. S., Berntsen, T. K., Godal, O., Sausen, R., Shine, K. P., and Skodvin, T.: Metrics of climate
 539 change: Assessing radiative forcing and emission indices, *Climatic Change*, 58, 267-331, 2003.
- 540 Fuglestedt, J. S., Shine, K. P., Berntsen, T., Cook, J., Lee, D. S., Stenke, A., Skeie, R. B., Velders, G. J. M., and
 541 Waitz, I. A.: Transport impacts on atmosphere and climate: Metrics, *Atmospheric Environment*, 44, 4648-4677,
 542 2010.
- 543 Hewitt, H. T., Copley, D., Culverwell, I. D., Harris, C. M., Hill, R. S. R., Keen, A. B., McLaren, A. J., and
 544 Hunke, E. C.: Design and implementation of the infrastructure of HadGEM3: the next-generation Met Office
 545 climate modelling system, *Geosci. Model Dev.*, 4, 223-253, 10.5194/gmd-4-223-2011, 2011.
- 546 IPCC: The Physical Science Basis. Contribution of Working Group I to the Fifth Assessment Report of the
 547 Intergovernmental Panel on Climate Change, edited by: Stocker, T. F., Qin, D., Plattner, G. K., Tignor, M.,
 548 Allen, S. K., Boschung, J., Nauels, A., Xia, Y., Bex, V., and Midgley, P. M., Cambridge University Press,
 549 Cambridge, United Kingdom and New York, NY, USA, 1535 pp., 2013.
- 550 Iversen, T., Bentsen, M., Bethke, I., Debernard, J. B., Kirkevåg, A., Seland, Ø., Drange, H., Kristjánsson, J. E.,
 551 Medhaug, I., Sand, M., and Seierstad, I. A.: The Norwegian Earth System Model, NorESM1-M – Part 2: Climate
 552 response and scenario projections, *Geosci. Model Dev.*, 6, 389-415, 10.5194/gmd-6-389-2013, 2013.
- 553 Klimont, Z., Höglund-Isaksson, L., Heyes, C., Rafaj, P., Schöpp, W., Cofala, J., Purohit, P., Borken-Kleeefeld, J.,
 554 Kupiainen, K., Kiesewetter, G., Winiwarter, W., Amann, M., Zhao, B., Wang, S. X., Bertok, I., and Sander, R.:
 555 Global scenarios of air pollutants and methane: 1990-2050, In prep.
- 556 Lund, M., Berntsen, T., Fuglestedt, J., Ponater, M., and Shine, K.: How much information is lost by using
 557 global-mean climate metrics? an example using the transport sector, *Climatic Change*, 113, 949-963,
 558 10.1007/s10584-011-0391-3, 2012.
- 559 Lund, M. T., Berntsen, T. K., Heyes, C., Klimont, Z., and Samset, B. H.: Global and regional climate impacts of
 560 black carbon and co-emitted species from the on-road diesel sector, *Atmospheric Environment*, 98, 50-58,
 561 <http://dx.doi.org/10.1016/j.atmosenv.2014.08.033>, 2014.
- 562 Myhre, G., Highwood, E., Shine, K. P., and Stordal, F.: New estimates of radiative forcing due to well mixed
 563 greenhouse gases, *Geophysical Research Letters*, 25, 2715-2718, 1998.
- 564 Myhre, G., Berglen, T. F., Johnsrud, M., Hoyle, C. R., Berntsen, T. K., Christopher, S. A., Fahey, D. W.,
 565 Isaksen, I. S. A., Jones, T. A., Kahn, R. A., Loeb, N., Quinn, P., Remer, L., Schwarz, J. P., and Yttri, K. E.:
 566 Modelled radiative forcing of the direct aerosol effect with multi-observation evaluation, *Atmos. Chem. Phys.*, 9,
 1365-1392, 10.5194/acp-9-1365-2009, 2009.



- 568 Myhre, G., Shindell, D., Bréon, F.-M., Collins, B., Fuglestedt, J. S., Huang, J., Koch, D., Lamarque, J.-F., Lee,
569 D., Mendoza, B., Nakajima, T., Robock, A., Stephens, G., Takemura, T., and Zhang, H.: Anthropogenic and
570 Natural Radiative Forcing, in: *Climate Change 2013: The Physical Science Basis. Contribution of Working
571 Group I to the Fifth Assessment Report of the Intergovernmental Panel on Climate Change*, edited by: Stocker,
572 T. F., Qin, D., Plattner, G. K., Tignor, M., Allen, S. K., Boschung, J., Nauels, A., Xia, Y., Bex, V., and Midgley,
573 P. M., Cambridge University Press, Cambridge, United Kingdom and New York, NY, USA, 2013.
- 574 Najafi, M. R., Zwiers, F. W., and Gillett, N. P.: Attribution of Arctic temperature change to greenhouse-gas and
575 aerosol influences, *Nature Clim. Change*, 5, 246-249, 10.1038/nclimate2524, 2015.
- 576 Olivie, D. J. L., and Peters, G.: Variation in emission metrics due to variation in CO₂ and temperature impulse
577 response functions, *Earth System Dynamics*, 4, 267-286, 10.5194/esd-4-267-2013, 2013.
- 578 Samset, B. H., and Myhre, G.: Vertical dependence of black carbon, sulphate and biomass burning aerosol
579 radiative forcing, *Geophysical Research Letters*, 38, L24802, 10.1029/2011GL049697, 2011.
- 580 Sand, M., Berntsen, T. K., Seland, Ø., and Kristjansson, J. E.: Arctic surface temperature change to emissions of
581 black carbon within Arctic or midlatitudes, *Journal of Geophysical Research: Atmospheres*, 118, 7788-7798,
582 10.1002/jgrd.50613, 2013.
- 583 Schmale, J., Shindell, D., von Schneidmesser, E., Chabay, I., and Lawrence, M.: Clean up our skies, *Nature*,
584 515, 335-337, 2014.
- 585 Shindell, D., and Faluvegi, G.: Climate response to regional radiative forcing during the twentieth century,
586 *Nature Geoscience*, 2, 294-300, 2009.
- 587 Shindell, D., and Faluvegi, G.: The net climate impact of coal-fired power plant emissions, *Atmos. Chem. Phys.*,
588 10, 3247-3260, 10.5194/acp-10-3247-2010, 2010.
- 589 Shindell, D., Kuylenstierna, J. C. I., Vignati, E., van Dingenen, R., Amann, M., Klimont, Z., Anenberg, S. C.,
590 Muller, N., Janssens-Maenhout, G., Raes, F., Schwartz, J., Faluvegi, G., Pozzoli, L., Kupiainen, K., Höglund-
591 Isaksson, L., Emberson, L., Streets, D., Ramanathan, V., Hicks, K., Oanh, N. T. K., Milly, G., Williams, M.,
592 Demkine, V., and Fowler, D.: Simultaneously Mitigating Near-Term Climate Change and Improving Human
593 Health and Food Security, *Science*, 335, 183-189, 10.1126/science.1210026, 2012.
- 594 Shindell, D. T.: Evaluation of the absolute regional temperature potential, *Atmos. Chem. Phys.*, 12, 7955-7960,
595 10.5194/acpd-12-7955-2012, 2012.
- 596 Shindell, D. T.: Inhomogeneous forcing and transient climate sensitivity, *Nature Clim. Change*, 4, 274-277,
597 10.1038/nclimate2136, 2014.
- 598 Shine, K. P., Fuglestedt, J. S., Hailemariam, K., and Stuber, N.: Alternatives to the Global Warming Potential
599 for Comparing Climate Impacts of Emissions of Greenhouse Gases, *Climatic Change*, 68, 281-302,
600 10.1007/s10584-005-1146-9, 2005.
- 601 Stevens, B., Giorgetta, M., Esch, M., Mauritsen, T., Crueger, T., Rast, S., Salzmann, M., Schmidt, H., Bader, J.,
602 Block, K., Brokopf, R., Fast, I., Kinne, S., Kornblueh, L., Lohmann, U., Pincus, R., Reichler, T., and Roeckner,
603 E.: Atmospheric component of the MPI-M Earth System Model: ECHAM6, *Journal of Advances in Modeling
604 Earth Systems*, 5, 146-172, 10.1002/jame.20015, 2013.
- 605 Stevenson, D. S., Doherty, R. M., Sanderson, M. G., Collins, W. J., Johnson, C. E., and Derwent, R. G.:
606 Radiative forcing from aircraft NO_x emissions: Mechanisms and seasonal dependence, *J. Geophys. Res.*, 109,
607 D17307, 10.1029/2004jd004759, 2004.
- 608 Stohl, A., Aamaas, B., Amann, M., Baker, L. H., Bellouin, N., Berntsen, T. K., Boucher, O., Cherian, R.,
609 Collins, W., Daskalakis, N., Dusinska, M., Eckhardt, S., Fuglestedt, J. S., Harju, M., Heyes, C., Hodnebrog, O.,
610 Hao, J., Im, U., Kanakidou, M., Klimont, Z., Kupiainen, K., Law, K. S., Lund, M. T., Maas, R., MacIntosh, C.
611 R., Myhre, G., Myriokefalitakis, S., Olivie, D., Quaas, J., Quennehen, B., Raut, J.-C., Rumbold, S. T., Samset, B.
612 H., Schulz, M., Seland, O., Shine, K. P., Skeie, R. B., Wang, S., Yttri, K. E., and Zhu, T.: Evaluating the climate
613 and air quality impacts of short-lived pollutants, *Atmospheric Chemistry and Physics*, 15, 10529-10566,
614 10.5194/acp-15-10529-2015, 2015.
- 615 Søvdde, O. A., Gauss, M., Smyshlyayev, S. P., and Isaksen, I. S. A.: Evaluation of the chemical transport model
616 Oslo CTM2 with focus on arctic winter ozone depletion, *Journal of Geophysical Research: Atmospheres*, 113,
617 D09304, 10.1029/2007JD009240, 2008.
- 618 Tol, R. S. J., Berntsen, T., O'Neill, B. C., Fuglestedt, J. S., and Shine, K.: A unifying framework for metrics for
619 aggregating the climate effect of different emissions *Environmental Research Letters*, 7, 044006, 10.1088/1748-
620 9326/7/4/044006, 2012.
- 621 Wild, O., Prather, M. J., and Akimoto, H.: Indirect long-term global radiative cooling from NO_x emissions,
622 *Geophys. Res. Lett.*, 28, 1719-1722, 10.1029/2000gl012573, 2001.

623

624

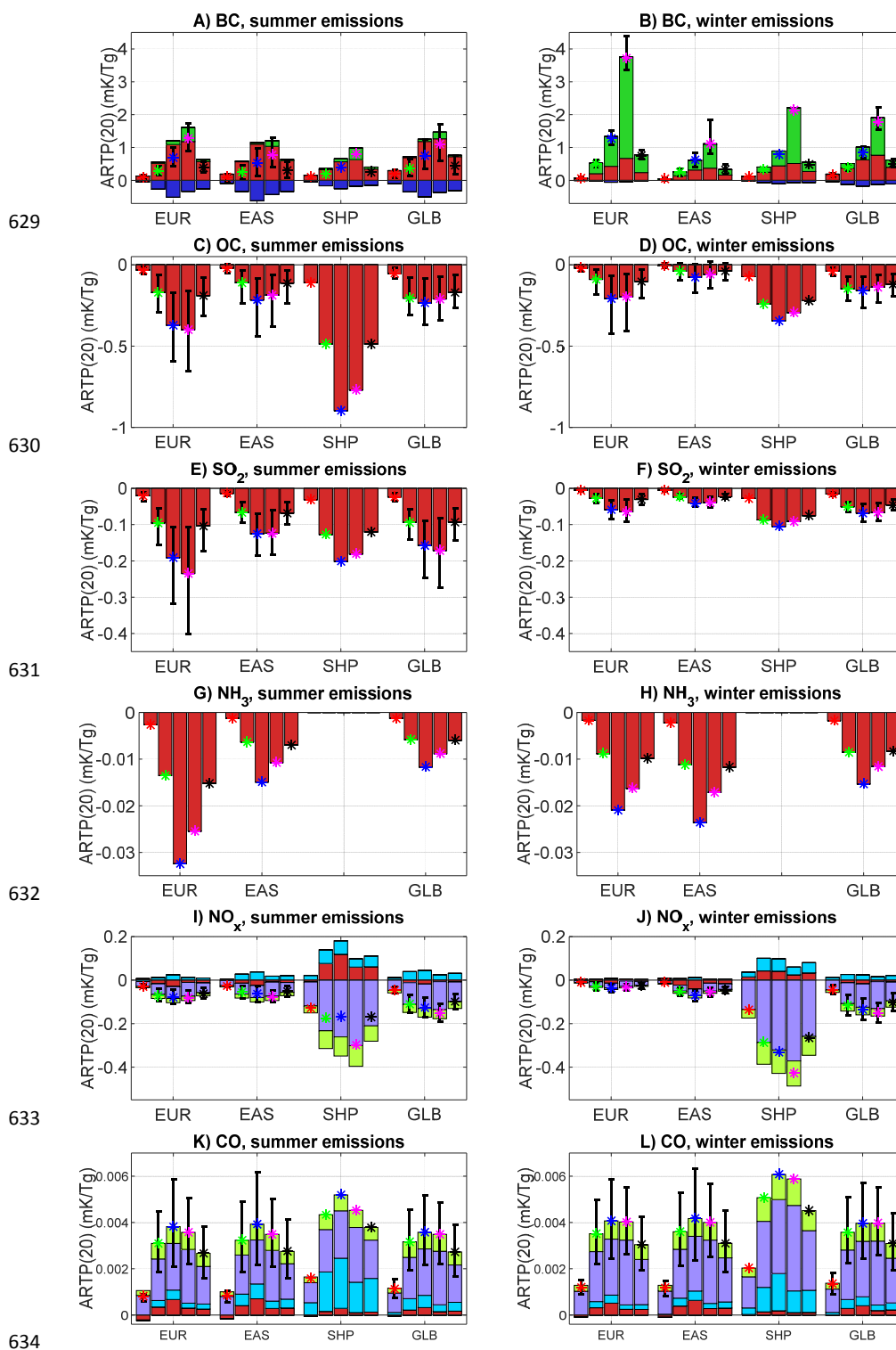


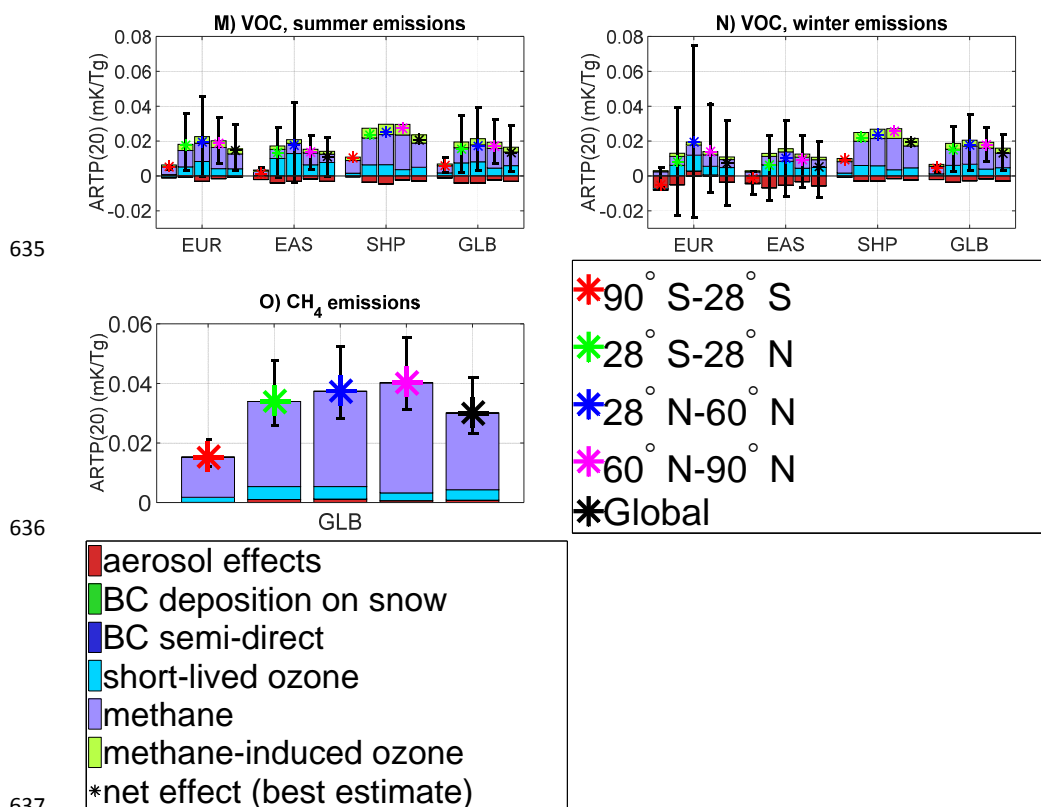
625 Table 1: The models and species included. Models are either general circulation models (GCM) or chemistry transport models
 626 (CTM). The resolution column shows the horizontal resolution and the number of vertical layers.

Model	Type	Resolution	BC	OC	SO ₂	NH ₃	NO _x	CO	VOC	CH ₄	References
ECHAM6-HAMMOZ	GCM	1.8°x1.8° L31	X	X	X						Stevens et al. (2013)
HadGEM3-GLOMAP	GCM	1.8°x1.2° L38	X	X	X		X	X	X	X	Hewitt et al. (2011)
NorESM	GCM	1.9°x2.5° L26	X	X	X		X	X	X	X	Bentsen et al. (2013); Iversen et al. (2013)
OsloCTM2	CTM	2.8°x2.8° L60	X	X	X	X	X	X	X	X	Søvde et al. (2008); Myhre et al. (2009)

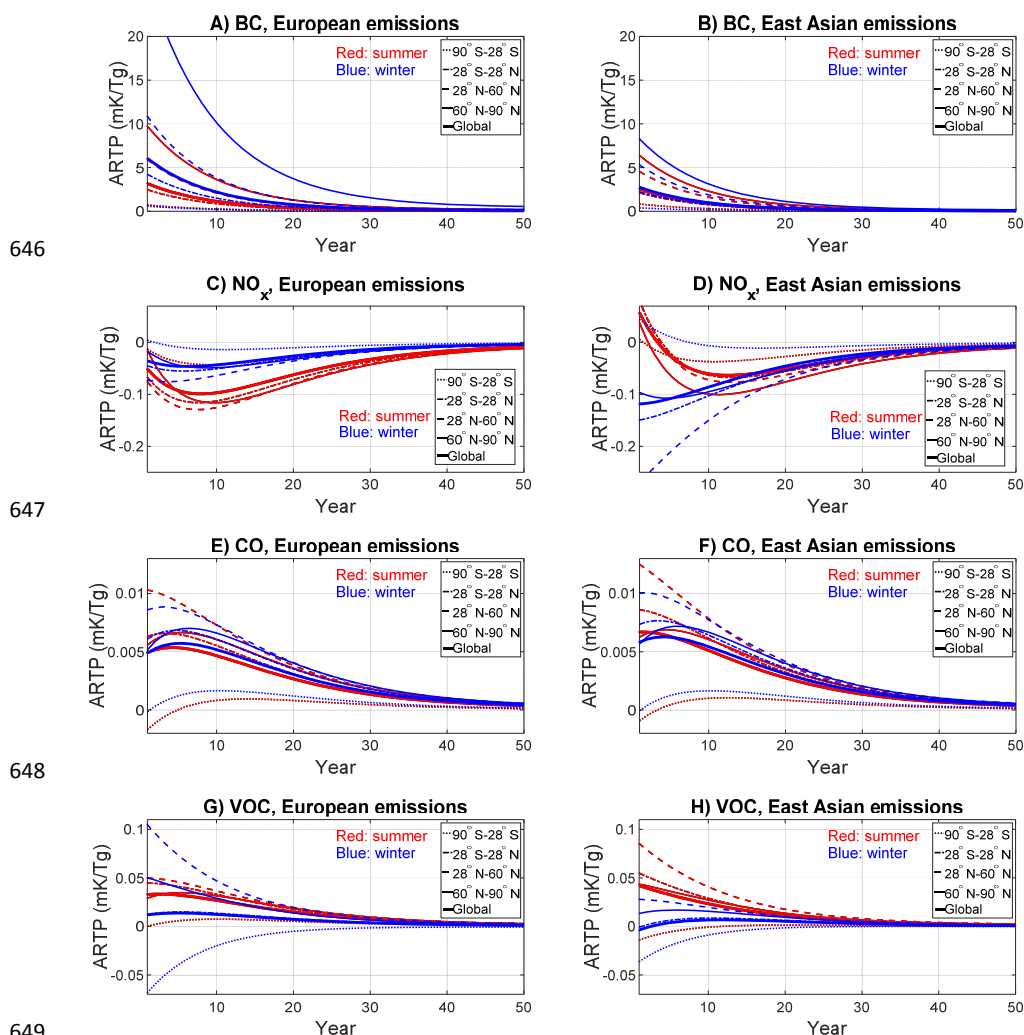
627

628



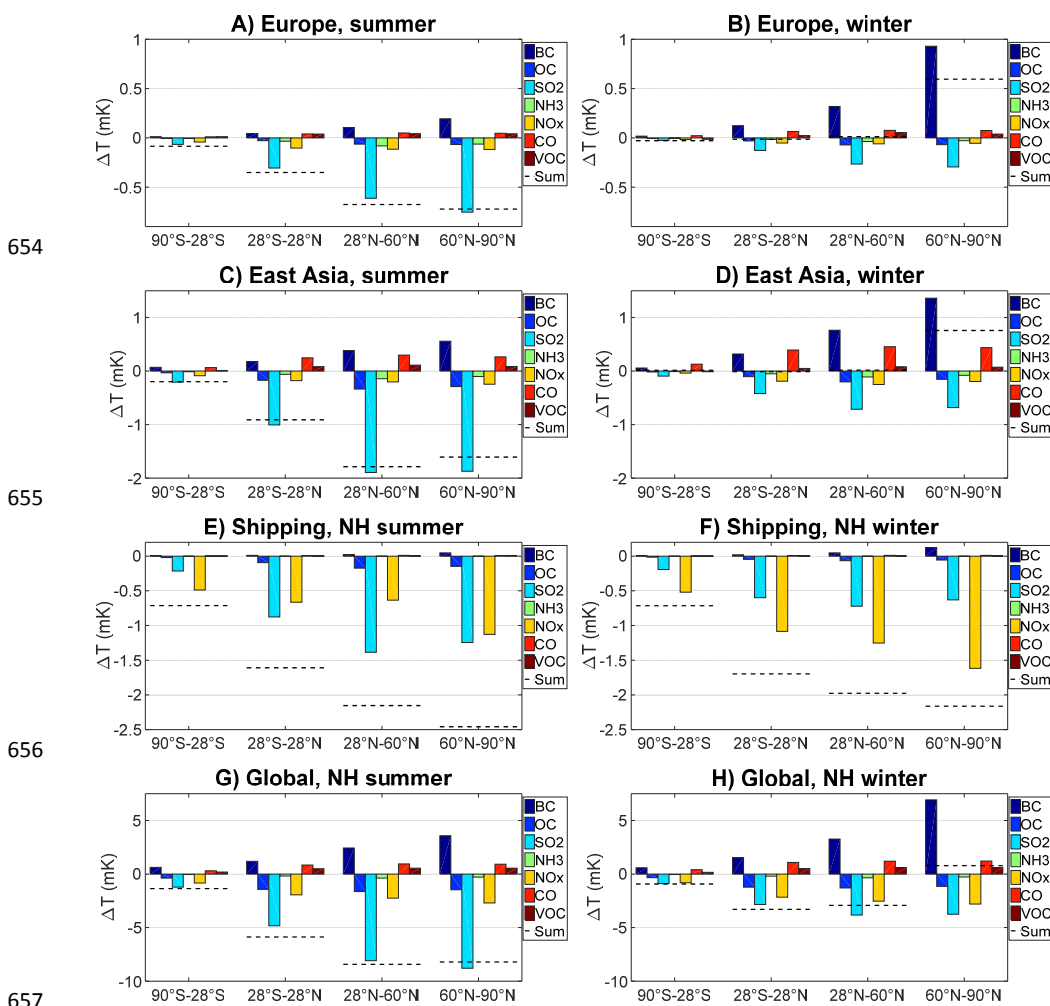


638 Figure 1: ARTP20 for emissions from Europe, East Asia, shipping, and global and for summer and winter. In each frame, and
 639 for each emission region, the ARTP20 values for the four latitudinal response bands from south (left) to north (right), as well
 640 as the global response average (rightmost), for the species, decomposed by processes. The net response is shown by the asterisk.
 641 The regions included are Europe (EUR), East Asia (EAS), shipping (SHIP), and global (GLB), all for both NH summer, May-
 642 October (left), and NH winter, November-April (right). The uncertainty bars show the range across models, which is not given
 643 for shipping as the best estimate is based on only two models for that sector. Due to the methodology applied, a fraction of the
 644 semi-direct effect for BC in the Arctic is included in the *aerosol effects* process, as explained in Sect. 2.2.4. Note that the
 645 vertical axis varies between different emitted components.



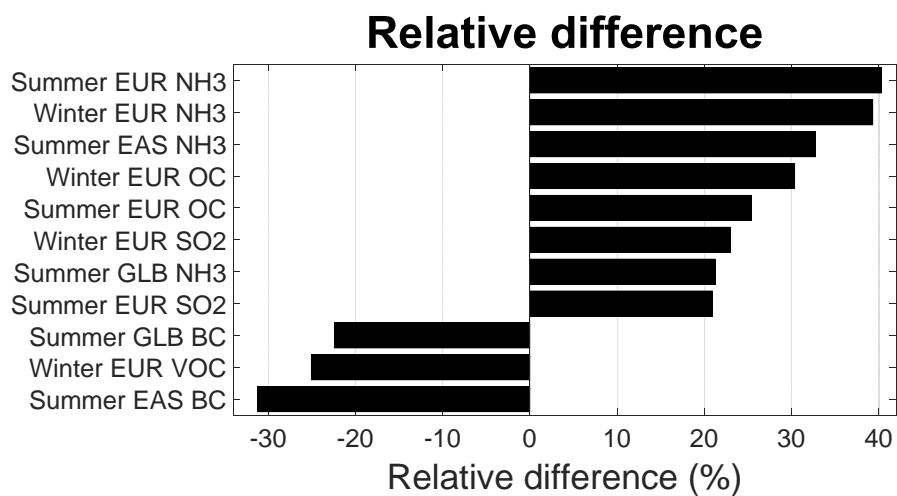
650 Figure 2: ARTP values in different response bands for BC and the ozone precursors for time horizons up to 50 years. Emissions
651 in Europe (left) and East Asia (right) in NH summer (May-October) are given as red and in NH winter (November-April) as
652 blue.

653



658 Figure 3: The regional temperature response for a time horizon of 20 years after regional and seasonal emissions in 2008 based
 659 on ARTP(20). The four latitude response bands represent the SH mid-high latitudes, Tropics, NH mid-latitudes, and Arctic.
 660 The global response average is given in Fig. S2. From top to bottom, the emission regions are Europe, East Asia, the global
 661 shipping sector, and global. The emissions are split into NH summer season (May-October) to the left and NH winter season
 662 (November-April) to the right. Note that the y-axis differs for the regions. The horizontal dashed lines show the sum for each
 663 response band.

664



665

666 Figure 4: The relative difference between the global temperature responses based on ARTP and AGTP methods for a time
667 horizon of 20 years. Only cases with larger relative differences than 20% are shown. Positive numbers occur when the
668 magnitude of the global temperature response is larger when based on ARTP than on AGTP, negative when the magnitude is
669 largest based on AGTP.

670